ISET Journal of Earthquake Technology, Paper No. 507, Vol. 47, No. 1, March 2010, pp. 1–23

TECOMÁN EARTHQUAKE: PHYSICAL IMPLICATIONS OF SEISMIC SOURCE MODELING, APPLYING THE EMPIRICAL GREEN'S FUNCTION METHOD, AND EVIDENCE OF NONLINEAR BEHAVIOR OF GROUND

Alejandro Ramírez-Gaytán*, Jorge Aguirre** and Carlos I. Huerta-López***

*Geological Sciences Department, San Diego State University
San Diego, CA 92182-1020, U.S.A.
**Instituto de Ingeniería, Universidad Nacional Autónoma de México
04510 México, D.F., Mexico
***Civil Engineering and Surveying Department, University of Puerto Rico at Mayaguez
Mayagüez, PR 00681-8041, U.S.A.

ABSTRACT

In this study, we generate a source model for the Tecomán Mexico earthquake of January 22, 2003. The presence of soft soils and the location of eight of the ten major cities of Colima state in its earthquake prone area are important factors to model the seismic source. We model in the frequency interval of 1–10 Hz, because many buildings, bridges and civil construction have their dominant vibration periods in this range. For generating the model, we apply the empirical Green's function method (EGFM) considering the Tecomán earthquake (M_W = 7.5) as the target event and the November 19, 2006 (M_W = 5.5) earthquake as the element event. At the recording site of MANZ, we did a spectral analysis to compare weak and strong ground motions in order to identify if some energy distribution is biased and concentrated at certain frequencies in the frequency interval of 1–10 Hz. The synthetic waveforms and Fourier spectra show good fitting with the observed ones at five stations. The latter roughly correspond to the dislocation model found by Yagi et al. (2004).

KEYWORDS: Empirical Green's Function Method (EGFM), Manzanillo Recording Station (MANZ), Target Event, Element Event

INTRODUCTION

Colima, due to its location, is one of the states of Mexico that are subjected to the occurrences of destructive earthquakes. Much of this seismicity has originated in the subduction zone, along the Pacific coast of Mexico. Although the rate of seismicity is lower than that in the state of Guerrero, it is not negligible. Two examples are the earthquakes of 1932 (M_W = 8.0) and 2003 (M_W = 7.5) (see Figure 1), which are the largest earthquakes recorded throughout Mexico during the last and present century, respectively.

The instrumentation and seismicity in the state did not receive adequate attention, and until 2005 Colima had only a single accelerograph station. Although Red Sísmica del Estado de Colima (RESCO) was operating, its network was installed with the purpose of monitoring the activity of the Colima volcano, and it did not produce useful records since all of them were saturated during the Tecomán earthquake. Thus, the investigations have been made only based on teleseismic and regional records (dominated by low frequencies), to determine the source model of the two largest earthquakes that have affected the region. However, the absence of accelerographic and wide-band networks inside Colima does not permit us to tackle source models in high frequencies.

Yagi et al. (2004) generated a source model that showed a clear directivity towards inside the state (i.e., El Gordo graben and Colima graben). Zobin and Pizano-Silva (2007) also showed directivity in the same zone. In these areas, the Tecomán earthquake (M_W = 7.5) produced more damage than the Manzanillo earthquake (October 9, 1995; M_W = 8.0). Therefore, it is important to generate a source model in high frequencies that can be used in future to estimate high-acceleration records in the area affected by the directivity of the Tecomán earthquake. It is useful in seismic engineering to recover the

histories of acceleration because many structures have natural periods in the high-frequency range (1–10 Hz). We took the first step to reach this objective in this study: the use of available data to generate a source model.

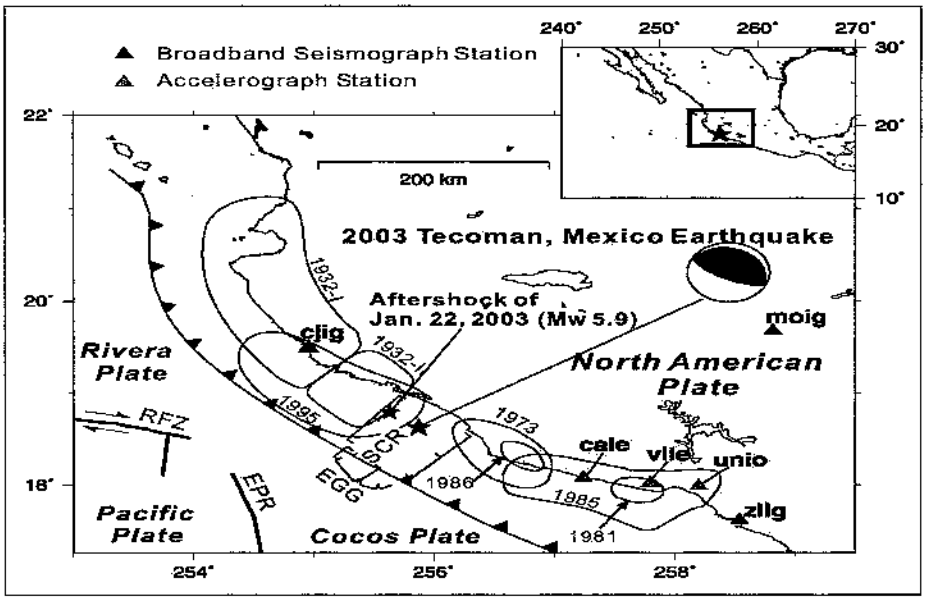

Fig. 1 Geographic map showing the location and rupture area of the major earthquakes that occurred in the region (from Yagi et al., 2004)

Five stations were used for modeling the seismic source of the Tecomán earthquake (January 22, 2003; M_W = 7.5). The local condition of the MANZ site is alluvial soft soil and the maximum acceleration recorded at this site is 0.37*g*. Due to these two particular conditions, an immediate doubt arises whether the site responded with a significant nonlinear behavior in the frequency interval of 1–10 Hz, which is our frequency band of interest.

In order to solve the lack of instrumentation in the region, we initiated a project whose main objective was to set up instruments permanently in Colima. For this purpose, we installed a temporary network consisting of 16 accelerographs and 9 short-band seismographs. All instruments were installed along the 120-km long coastline and inside the Colima state. The data recorded by this network can be used in future to simulate the peak ground acceleration and time-histories of the ground acceleration during the Tecomán earthquake. However, in this study we tried to take the first step: to generate a source model.

As a result of the instrumentation work, on November 19, 2006, this network recorded the most important event since the earthquake of 2003. Its epicenter can be seen in Figure 2. This earthquake was recorded at 16 acceleration stations and 9 velocity stations of the temporary network installed as part of the project. This event was located within the rupture area of the Tecomán earthquake (of January, 2003). In addition to our network, this was recorded by the local acceleration station in Manzanillo (MANZ) and four velocity-type broad-band stations of Servicio Sismológico Nacional (SSN), which are the same stations that recorded the Tecomán earthquake. The features mentioned above allow the application of the empirical Green's function method proposed by Irikura (1986), by using the earthquake of November 19, 2006, to simulate the Tecomán earthquake.

We estimated the strong motion generation areas (SMGAs) by using this method and the frequency band of 1–10 Hz, which corresponds to high frequencies that cannot be modeled by other theoretical approaches, due to the lack of cortical structure information. The SMGAs are rectangular areas where the slip exceeds the average slip of the fault; it is considered that in this area the slip, stress drop, and rupture velocity are constants (Miyake et al., 2003). This simple source model has been successfully applied to simulate acceleration records of some moderate and large earthquakes. However, unlike the SMGAs, the asperities are estimated through inversions using low frequencies in the 0.1–0.5 Hz range. An asperity is defined as a region within the dislocation area, in which the slip exceeds the average slip in the entire dislocation area (Somerville et al., 1999).

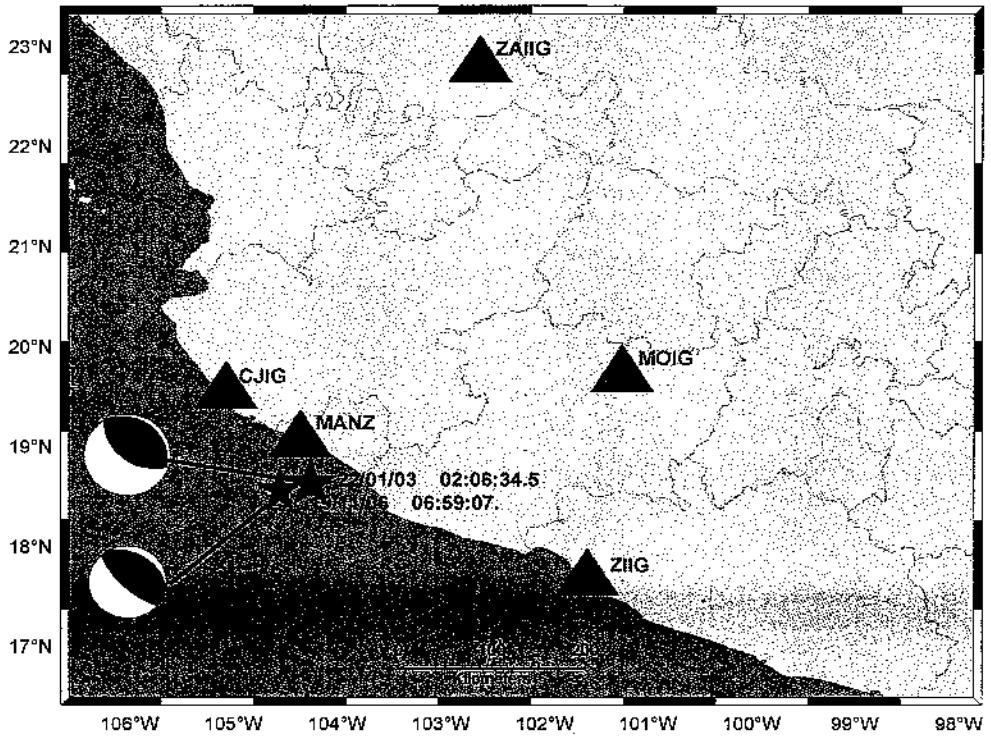

Fig. 2 Geographic map showing the epicentral locations and focal mechanisms of the Tecomán earthquake and the event of November 19, 2006, along with the geographical locations of the local acceleration stations and regional stations that recorded both earthquakes

Miyake et al. (2003) showed that the SMGAs are located almost on the same positions as the asperities and that those match roughly the areas of highest dislocation or asperities, according to the criterion established by Somerville et al. (2002). Based on this criterion, the SMGAs found in our best model are compared with the dislocation model found by Yagi et al. (2004). Somerville et al. (1999) suggested that the dislocation for a subduction earthquake is characterized by a spatial variation of asperities in the dislocation area, and examined how the dislocation models are scaled with the seismic moment. Since our estimates of SMGAs approximately match the areas of highest dislocation or asperities, we quantified the characteristics of our SMGAs individually and as a whole to compare them with the relationships proposed by Somerville et al. (2002). It was found that these relationships are suitable to be applied to the subduction zone under study.

The fact that sediments can amplify earthquake ground motions was recognized at least 100 years ago (Milne, 1898). However, there has been a lingering uncertainty as to whether the degree of amplification varies with the level of input motion. This issue remains one of the most important questions with regard to understanding and predicting earthquake ground motions.

According to the energy conservation principle, seismic-wave amplitudes generally increase in sediments due to lower densities and/or lower seismic velocities. In addition, resonance effects can occur where abrupt impedance contrasts exist. If sediments were perfectly elastic, their response would be independent of the incident-wave amplitudes. As with any real material, however, sediments begin to yield at some level of strain, and this violation of the Hooke's law gives rise to nonlinear response.

The engineering community has long believed that sediment nonlinearity is significant. This perspective was based almost entirely on the laboratory studies, where observed stress-strain loops imply a reduced effective shear modulus and an increased damping (i.e., lower Q) at higher levels of strain. A reduced shear modulus alone implies an increased amplification, depending on how it is measured. However, the increased damping generally tends to dominate, thus resulting in a reduced amplification (and even possible de-amplification). One manifestation of this perspective was that peak ground acceleration (PGA) got reduced (or deamplified) at sediment sites when rock-site PGA exceeded 0.1g (Seed and Idriss, 1982). The 1985 Michoacán and 1989 Loma Prieta earthquakes however changed this perspective, by shifting the threshold between PGA amplification and deamplification to ~0.4g for deep,

soft clay sites (Finn, 1991; Idriss, 1990). Furthermore, the data obtained during the 1989 Loma Prieta and 1994 Northridge earthquakes indicated a threshold of ~0.6g for deep, stiff soil sites (Chang and Bray, 1998).

On the other hand, seismologists have traditionally been skeptical of the significance of sediment nonlinearity, in spite of the fact that one of their very own (Reid, 1910) recognized and described the potential effect some 90 years ago (in the same paper that introduced the elastic-rebound theory of faulting). The prevailing seismological perspective as of 1988 was reflected in a seminal review paper by Aki (1988), who wrote, "... except for the obvious case of liquefaction, ... the amplification factor obtained using weak motion data can be used to predict ... strong ground motion ...". The reason for this view was either that nonlinear effects were indeed insignificant, or that they could not be resolved among the myriad of other effects complicating a very limited number of strong-motion observations. Seismologists were also skeptical that laboratory studies reflect the 'in situ' behavior, both because of the well-known difficulties in obtaining undisturbed samples, and because such studies do not include the effects of scattering attenuation. Given a lack of direct evidence for sediment nonlinearity, seismologists naturally opted for the simpler linear model (which is also generally more conservative in terms of the predicted ground motion). Keiiti Aki turned out to be one of the earliest seismological converts. In a follow-up review paper, he wrote, "Non-linear amplification at sediment sites appears to be more pervasive than seismologists used to think" (Aki, 1993).

A published seismological study claims to have identified a pervasive nonlinear effect (Field et al., 1997); and sediment amplification factors were inferred from the 1994 Northridge earthquake main shock, which were up to a factor of two less, on average, than for the relatively weak-motion aftershocks. Although this nonlinear interpretation seems to be most reasonable, it remains to be seen whether the conclusion holds up to an additional scrutiny. Given the recent progress, the time is ripe to reassess our present understanding (or, lack thereof) with respect to the nonlinear sediment response. In general terms, Hooke's law is only an approximation, especially because some degree of nonlinearity is apparent in laboratory studies at even the lowest detectable strain levels. The question is more of degree, or of the adequacy of the linear model under various conditions, especially in comparison with the other commonly made approximations (such as isotropy). In other words, when is sediment nonlinearity a first-order effect in terms of understanding or predicting earthquake ground motions?

Based on the statements published in several papers related to nonlinear effects, we have carried out a spectral analysis comparing weak, moderate, and strong ground motions as an alternate way to identify empirically if some energy is concentrated at particular frequencies (which may be used as an indicator of the nonlinear effects) in the frequency interval of 1–10 Hz for the MANZ site. This alternative is adopted here because a detailed nonlinear analysis is a different kind of study, which is out of the context of our research.

TECTONIC AND HISTORICAL SEISMICITY

There are three seismic sources in the state of Colima. The first source is the Colima volcano that generates microtremors and low-magnitude earthquakes (of magnitudes generally less than 3.5). The second source comes from the seismic block of Jalisco, which is located in the North American plate and borders on the east with the Rivera plate, southward with the El Gordo graben and the Colima graben, and in the north with the graben of Tepic and Chapala (Bandy et al., 1995). In this region there have been significant intraplate earthquakes with magnitudes not greater than 6.0. In our temporary seismic network, we recorded a significant seismic activity in this area, which seems to be cut exactly on the limits between the El Gordo graben and the block of Jalisco.

The most important seismic source in the region is the subduction zone, located in front of the coast of the state of Colima, where the Rivera, Cocos and North America plates converge. The Cocos and Rivera plates are subducting under the North American plate at an average rate of 5 cm per year. This mechanism occurs in front of the coast of the state in the area known as El Gordo graben (see Figure 1).

The Tecomán earthquake occurred in the seismic gap that forms the boundaries of the rupture area of the 1973 and 1995 earthquakes. However, the location of the aftershocks of the Tecomán earthquake indicates that their rupture area covers the northern part of the El Gordo graben and invades part of the rupture zone of the 1932 and 1995 earthquakes. The absence of aftershocks in the southwest indicates that half of this seismic gap was not broken (Quintanar et al., 2010).

An analysis of the data presented in Table 1 shows that the 1995 and 1932 earthquakes, although they had different rupture areas, had the same M_W (equal to 8.0). This indicates that the earthquake of 1995 released an amount of energy equivalent to that of the largest recorded earthquake in the history of Mexico.

Table 1: Location Data, Magnitude and Seismic Moment of Main Earthquake Occurrences in the Region

Date	Latitude	Longitude	M_0 (N-m)	M_W
1932 06 03	19.80°	−104.00°	9.1×10^{20}	8.0*
1932 06 18	18.95°	−104.42°	7.3×10^{20}	7.9*
1973 01 30	18.39°	−103.21°	3×10^{20}	7.6+
1995 10 09	19.05°	−104.20°	9.1×10^{20}	8.0**
2003 01 22	18.625°	−104.12°	1.6×10^{20}	7.5**

*Singh et al. (1985); +Alcocer and Klingner (2006); **Harvard CMT[1]

The big difference between the seismic moments of the 1995 earthquake ($M_0 = 9.0\times10^{20}$ N-m) and the Tecomán earthquake ($M_0 = 1.6\times10^{20}$ N-m) shows that the Tecomán earthquake had much less energy than the earthquake of 1995. However, the damage caused by the Tecomán earthquake was much higher in the urban areas of the state with the exception of Manzanillo city. Directivity is one of the reasons that can explain this phenomenon. The earthquake directivity towards the interior of the North American plate coincides with the geographical locations of eight of the ten largest urban areas in the state. Because these urban areas along with the earthquake rupture direction are located within the Colima graben, it is important in future projects to explore the role of this graben in the conduction of seismic energy (through the transmission, reflection and refraction of waves) produced by this source. The site effects produced by the alluvial or dilluvial deposits within the graben also have to be considered. These two phenomena together could be responsible for the large accelerations in the area. The difference between the seismic moments of the 1995 and 2003 earthquakes, which share a zone of rupture area, suggests that if an earthquake of similar magnitude to the 1995 earthquake occurs in the portion of the seismic gap inside the Colima graben, going by the above-explained causes it would create a very critical seismic scenario for the region.

DATA

We collected records from the main shock of January 22, 2003 (i.e., the target event) and the earthquake of November 19, 2006 (i.e., the element event), both recorded at the accelerograph station MANZ (see Figure 2), which is owned by Federal Electricity Commission (CFE) and operated by Centro de Instrumentación y Registro Sísmico (CIRES). This station is located 54 km away from the epicenter and is the nearest accelerograph station that recorded the Tecomán earthquake. The equipment is a DCA-333 three-component accelerograph that records the acceleration waveform with 100 samples per second and has a trigger threshold of 4.9 gal (0.049 m/s^2).

Attempts were made to collect acceleration records for both events from the stations of Servicio Sismológico Nacional (SSN) with good azimuthal coverage around the target event and those stations are Chamela (CJIG), Morelia (MOIG), Zacatecas (ZAIG), and Zihuatanejo (ZIIG) (see Figure 2). According to the information provided by the staff of SSN, the acceleration records were not stored in memory, in contrast with the velocity records that are stored in memory. For this reason we had to work with the velocity records. The four stations being considered have broad-band seismographs: those at the stations CJIG and ZIIG have a sampling rate of 80 samples per second, while those at the stations MOIG and ZAIG have a sampling rate of 100 samples per second. The data was first changed from the original format to the ASCII format and was subsequently converted from velocity to acceleration.

The focal mechanisms adopted for the main shock and secondary earthquake are same as those reported by Harvard CMT[1], i.e., strike 308°, dip 12°, and slip 110° for the main shock, and strike 300°, dip 21°, and slip 74° for the secondary earthquake (see Table 2). The dislocation area is assumed to be 70×85 km which is same as in Yagi et al. (2004).

Table 2: Locations for Target and Element Events, as Determined by Servicio Sismológico Nacional (SSN), and Focal Mechanisms for Both Events, as Determined by Central Moment Tensor (CMT[1])

	Target Event	Element Event
Origin time (local time)	22/01/2003 02:06 GMT	19/11/2006 06:59
Hypocentral location (latitude, longitude, and depth)	(18.60°N, 104.22°W, 26 km)	(18.46°N, 104.49°W, 18 km)
Magnitude M_W	7.5	5.5
Focal mechanism (strike, dip, rake)	(308°, 12°, 110°)	(300°, 21°, 74°)

By using the accelerograms, we extracted the flat levels of displacement spectra for low frequencies and the flat levels of acceleration spectra for high frequencies for the MANZ station. Based on the analysis of these spectra, we discovered that the flat levels of acceleration spectra were between 1.0 and 10 Hz. Also, corner frequencies (i.e., the values of f_c) were obtained for the element and target events.

For the spectral analysis, background noise data was collected at four sites: MANZ, CASA, CAMPOS, and LAGO. Figure 3 shows the Google satellite image of the area and the locations of sites. In Table 3 the details of geographic locations and soil classifications are provided.

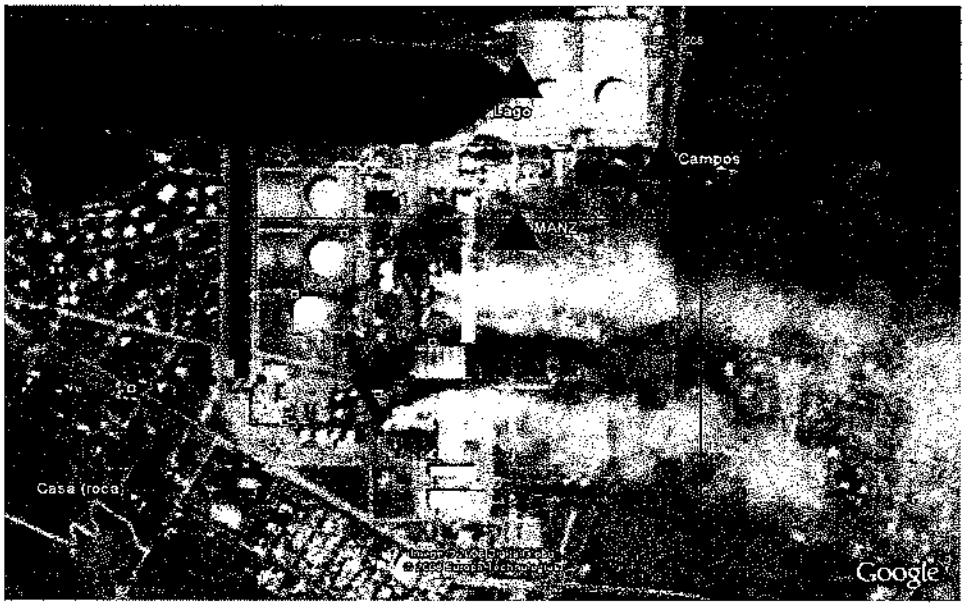

Fig. 3 Google satellite image of the area and the locations of sites (shown by the triangles) for the spectral analysis; background noise data was collected at four sites: MANZ (soil), CASA (rock), CAMPOS (soil), and LAGO (soil)

Table 3: Details of Geographic Locations and Soil Classifications for the Four Sites Considered to Collect Background Noise Data for the Spectral Analysis

Station	Latitude	Longitude	Time of Record (s)	Type of Soil
CAMPOS	19.0289°	−104.316°	31417 seg (8.7 hrs)	Soil
CASA	19.0236°	−104.325°	35553 seg (9.87 hrs)	Rock
MANZ	19.027710°	−104.318504°	34820 seg (9.67 hrs)	Soil
LAGO	19.030273°	−104.318581°	36001 seg (10.00 hrs)	Soil

Among the four sites considered, CASA is located in a rocky outcrop, and the other three in soft soils. We used two earthquake records, in addition to the above background time series, and those correspond to

the target and element events considered above; the epicenters of both events were close to each other (see Figure 2). The record lengths of the two ground motions were 2545 and 2565 sample points per channel respectively, and both ground motions were recorded at the soft-soil site at MANZ.

The background noise data was collected by using the Kinemetrics K2 recorders of 24-bit ADC converter, with integrated accelerometers of $2g$ at full scale, and three additional recording channels with externally connected Guralp-40T sensors. The sampling frequency was 100 Hz, together with unit gain.

Segments of ground motions for the background noise were plotted for visual inspection. The visual inspection was mainly concerned with the selection of desired types of signals for use in the frequency domain analysis, which consisted of power spectral density (PSD) estimations of the time series. For this we avoided those time periods which might contain signals due to seismic events and other transient signals. Significant differences in background noise levels were evident between the horizontal and vertical components.

For unit conversion from digital units (DU) to physical units of the background noise ground motion in velocity (in m/s), we used the Guralp-40T sensor conversion factor of 2000 V/m/s over the frequency band of 0.03–50 Hz. The D.C. offset was removed from the selected time series. The plots of the prepared time-series segments were useful to double-check the amplitude levels of the recorded background noise ground motions by comparison with the published data from similar studies. In computing PSD from the background noise, more stable and reliable PSD estimates were obtained with the use of larger ensembles of time series in the averaging process. For the background-noise analysis, we used time series of one hour length, which contained 360,000 sample points per channel. We excluded, either manually or by an implemented automatic algorithm, transient signals, if any, in obtaining the PSD spectra.

METHOD

The method used to model the target event (i.e., Tecomán earthquake of January 22, 2003 in this study) requires a small-magnitude earthquake (i.e., the earthquake of November 11, 2006 in this study) with its hypocenter near the hypocenter of the target event. On applying the synthetic method for the ω^{-2} spectral model, as proposed by Aki (1967), we obtain the necessary number of subevents, N^3, from the relationship between the seismic moments of the target event (to be simulated) and the element event, which is used as the empirical Green's function. When N^3 is equal to the number of sub-faults in the directions of strike (i.e., N_x), dip (i.e., N_w), and time (i.e., N_t), i.e.,

$$N^3 = N_x \times N_w \times N_t \tag{1}$$

it is necessary to find the parameter N used to scale the fault area of main event. Since it is divided into $N \times N$ sub-faults, N^3 is obtained as

$$\frac{\overline{U}_0}{\overline{u}_0} = \frac{M_0}{m_0} = N^3 \tag{2}$$

where $\overline{U}_0$ and $\overline{u}_0$ are the flat levels of the displacement Fourier spectra for the target and element events, respectively; and M_0 and m_0 are the seismic moments of the target and element events, respectively. The relationship for high frequency is given by

$$\frac{\overline{A}_0}{\overline{a}_0} = \left(\frac{M_0}{m_0}\right)^{1/3} = N \tag{3}$$

where $\overline{A}_0$ and $\overline{a}_0$ are the flat levels of the acceleration Fourier spectra of the target and element events, respectively.

Thus, the synthetic motion for the target event, $A(t)$, is given by that for the element event, $a(t)$, by using the following equations:

$$A(t) = \sum_{i=1}^{N_x} \sum_{j=1}^{N_w} \frac{r}{r_{ij}} F\left(t - t_{ij}\right) a(t) \tag{4}$$

$$F_{ij}\left(t-t_{ij}\right)=\delta\left(t-t_{ij}\right)+\frac{1}{n'}\sum_{k=1}^{(N-1)n'}\delta\left(t-t_{ij}-\frac{(k-1)\tau}{(N-1)n'}\right) \tag{5}$$

where n' is an appropriate value to eliminate spurious periodicity, r is the distance from the station to the element-event hypocenter, r_{ij} is the distance from the station to the subfault (i, j), and t_{ij} is the delay time of the rupture from the starting point (i, j) to the site of observation.

To use the element-event waveform with a different stress drop, the empirical Green's function formulation is modified by introducing a factor C that serves to correct the difference between the stress drops of the target and element events:

$$C=\Delta\sigma_{SP}/\Delta\sigma_{R} \tag{6}$$

The spectral levels of Equations (2) and (3) are affected by the same factor C as follows:

$$\bar{U}_0/\bar{u}_0=CN'^3 \tag{7}$$

$$\bar{A}_0/\bar{a}_0=CN' \tag{8}$$

Further, Equation (4) is amended by replacing $a(t)$ with $Ca(t)$ and N with N' as

$$A(t)=\sum_{i=1}^{N'}\sum_{j=1}^{N'}\frac{r}{r_{ij}}F(t_{ij})a(t) \tag{9}$$

For the spectral analysis, the data processing has followed the rules of Fourier analysis, as described, for example, in the books by Kanasewich (1981), Oppenheim and Shafer (1975), and Bendat and Piersol (1971). The PSD estimates for the background noise measurements have been obtained by using time series of 3600 s (with 360,000 samples) and by averaging 351 sub-segments of 1024 points each and with an overlap of 75% in length. The time-series lengths of 25.45 and 25.65 s were used for the two earthquakes with M_W = 7.5 and 5.5, respectively. The same segment length and overlap, as those used for the background noise, were used for the earthquake time series. For both kinds of records, the mean value of each sub-segment was removed and a Hanning window was applied to each sub-segment. The averaged PSD estimates were then normalized by multiplying with the frequency increment Δf and the amplitude scaling factor (which equals two due to the symmetry property of DFT) and by dividing by the number of data points, N. Finally, after the instrument correction was applied, the spectral amplitudes were transformed to the units of acceleration. The ω^2 factor was applied for acceleration conversion from the velocity records. By means of using weak (for microtremors), moderate (for the earthquake of M_W = 5.5), and strong (for the earthquake of M_W = 7.5) ground motions, H/V spectral ratios (HVSPR) were computed between each horizontal component and the vertical component in order to identify empirically whether local site effects were present. As indicator of the above, the HVSPR spectra were inspected for energy concentration at particular frequencies within the frequency interval of 1–10 Hz. This procedure is an alternate way to provide an empirical evidence to accept or reject the hypothesis that at the MANZ site, nonlinear local site effects were significant. It should be pointed out that an evidence of nonlinearity is shown by significant decreases in the frequencies of peak spectral ratios, corresponding to material softening, as the amplitude is increased. The observed shifts in peaks do not show any significant contributions in the frequency range of 1–10 Hz. These results provide constraints for future numerical modeling studies on strong ground motions during earthquakes.

MODEL

Since the stress drop is different for the target and element events, the above method was applied (see Equations (4)–(6)). Thus, we obtained the parameters, N' = 8 and C = 1.08. We also need to assume and vary some other parameters in order to simulate the acceleration records. Those parameters are rupture velocity, rise time, and the point where the rupture starts, among others.

On applying this modeling, we found little sensitivity of the synthetics to the rise-time variations. On the other hand, we found high sensitivity of the synthetics to the rupture-velocity variation, and to the size

of SMGA and its location inside the fault plane. By applying this method, we generated several models in which these parameters were varied. The corresponding iterations can be classified in four stages: the models with one, two, three, and four SMGAs. As shown in Figure 4, the SMGA area is divided into four parts and these areas are positioned on each point into the dislocation area until the entire area is covered. Each variation in the position of SMGA corresponds to single iteration. In this process, the rupture velocity, rise time, and radiation pattern were varied. The size of SMGA changes in the strike or dip direction, according to the azimuth of the station or stations that had poor adjustment. In others, the location of SMGA was varied by moving it close to the hypocenter and by increasing its rupture velocity, while trying to compact or expand the packets of some waves within the trace. Major iterations were made by taking into consideration the best adjustments in the first, second and third previous stages (i.e., the process based on discrimination and optimization to determine the best model). The parameters and tests described above were applied in each one of the three stages. The best model for each stage was determined by minimizing the residuals between the synthetic and observed waveforms.

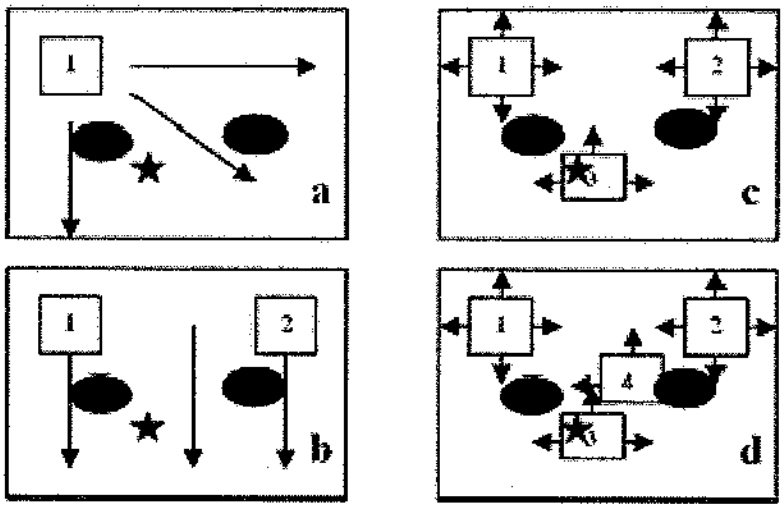

Fig. 4 Process of modeling in four stages for the Tecomán earthquake (oval: asperities of the dislocation model found by Yagi et al. (2004); star: epicenter of the Tecomán earthquake; numbered squares represent the SMGAs used in each stage; arrows show the direction of movement of each square searching the best residuals)

In the beginning, we modeled the target event by attempting to adjust the synthetics for the local station MANZ, and then by applying it to the regional stations. In the same way, some models were generated primarily by adjusting those to the waveforms for regional stations and then by applying those to the local station MANZ.

RESULTS

In the first stage, we modeled the target event by using one SMGA and by adjusting it to the source nearest to the MANZ station. The location of SMGA was varied around the fault plane. The best models were generated during the first stage when the only SMGA was located in the zones identified as SMGA "A" and SMGA "B" (see Figures 5(a) and 5(b)).

The first best-fit location (i.e., SMGA "A") was obtained when the target event was modeled with a SMGA of 59.16 km^2 and V_r = 2.1 km/s (see Table 4), located at 16.68 km SW from the hypocenter. The sum of residual values for each of the components in velocity, acceleration, and displacement for both models, which appear in Table 5, show a better match in the three components when modeling is done with one SMGA (i.e., SMGA "B") of 59.16 km^2 and V_r = 2.1 km/s (see Table 4), located at 21.27 km NE from the hypocenter (see Figure 5(a)).

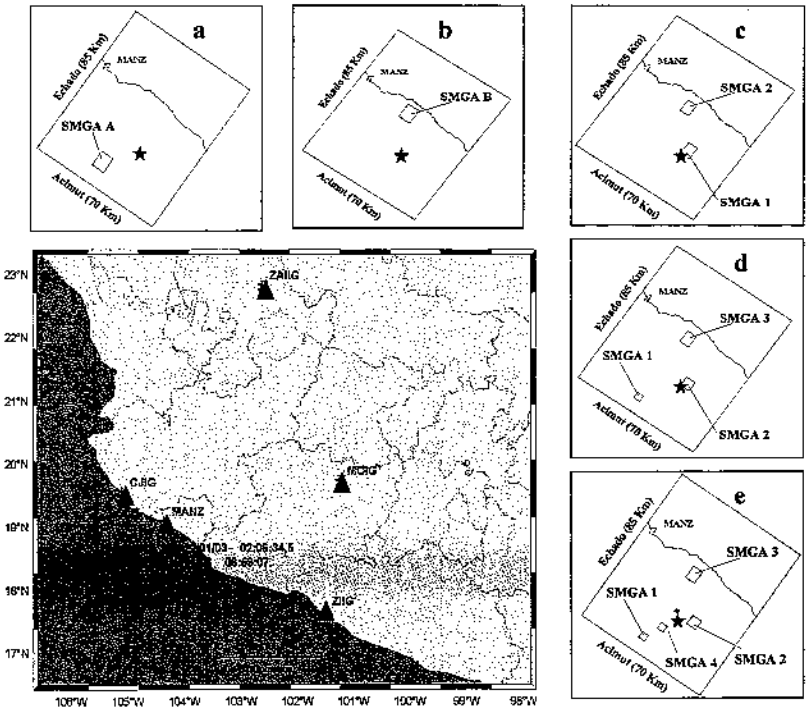

Fig. 5 Models with minor residuals generated in the EGFM process by using one SMGA (see (a) and (b)) and two, three and four SMGAs (see (c), (d) and (e), respectively)

Table 4: Locations and Areas of SMGAs for the Four Models Generated, with One, Two and Three SMGAs, Respectively, Where V_r is the Rupture Velocity

Model	SMGA	Length (km)	Width (km)	Area (km^2)	Starting Point of Rupture with Relation to Hypocenter	V_r (km/s)
1	1	8.60	6.88	59.168	16.68 km SW	2.1
2	1	8.60	6.88	59.168	21.27 km NE	2.1
3	1	5.16	6.88	35.5008	10.48 km SE	2.1
	2	5.16	6.88	35.5008	20.07 km NE	2.9
4	1	3.44	3.44	11.83	20.75 km SW	2.1
	2	5.16	5.16	26.62	10.24 km SE	2.9
	3	6.88	5.16	35.50	20.16 km NE	2.1
5	1	3.44	3.44	11.83	20.75 km SW	2.1
	2	5.16	5.16	26.62	10.24 km SE	2.9
	3	6.88	5.16	35.50	20.16 km NE	2.1
	4	3.44	3.44	11.83	18.45 km SW	2.9

Figure 6 (for SMGA "A") shows the comparisons between the observed records (see the bottom curves) and synthetic records (see the top curves) for the three components in velocity, acceleration, and displacement in the first stage.

In the second stage, the Tecomán earthquake of 2003 is modeled with two SMGAs. Here, we also adjusted the synthetic record to those recorded at the nearest station to the source (i.e., MANZ). The locations of the two SMGAs were varied within the fault plane. The model with the best fitting was applied to the records obtained from the regional stations, CJIG, MOIG, ZAIG, and ZIIG. These four regional stations provide a good azimuthal coverage around the earthquake. The residual values for three components in velocity, acceleration, and displacement presented in Table 5 show that the best fitting was obtained for the model shown in Figure 5(c). This model consists of one SMGA of 35.50 km^2 located at 10.48 km SE from the hypocenter, and another SMGA of 35.50 km^2, located at 20.07 km NE from the hypocenter as shown in Table 4.

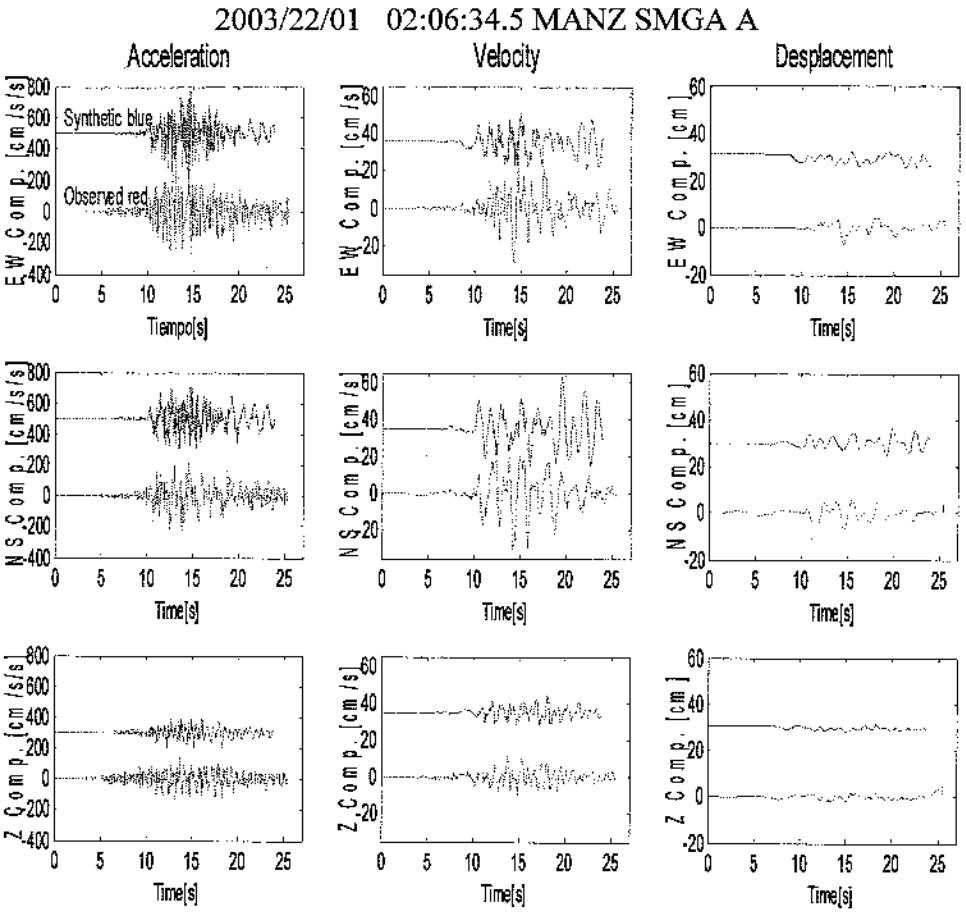

Fig. 6 Simulation for MANZ station with one SMGA (top: synthetic; bottom: observed; columns from left to right: acceleration, velocity, and displacement; rows from top to bottom: EW, NS, and Z components)

In the third stage, we modeled the target event with three SMGAs by adjusting the synthetic records to those recorded at the source of the nearest station (i.e., MANZ). The locations of these three SMGAs were varied within the fault plane. The best-fit model was also applied to the records from the regional stations, CJIG, MOIG, ZAIG and ZIIG. Table 5 shows that the best fitting was obtained for the model presented in Figure 5(d). This model consists of three SMGAs. One of them is 11.83 km^2, located 20.75 km SW from the hypocenter; another has 20.62 km^2, located 10.24 km SE from the hypocenter; and the third one has 35.50 km^2, located 20.16 km NE from the hypocenter. The features of this model are also listed in Table 4.

Table 5: Sum of Residuals for EW, NS and Z Components in Acceleration, Velocity and Displacement

Models for MANZ Station	**Residual**		
	Acceleration	**Velocity**	**Displacement**
One SMGA (SMGA "A")	108.75	29.62	9.55
One SMGA (SMGA "B")	23.00	12.50	7.05
Two SMGAs	6.13	17.32	5.63
Three SMGAs	4.79	3.36	4.59
Four SMGAs	6.82	6.92	10.44
Models for Regional Stations, CJIG, MOIG, ZAIG, ZIIG	**Average Residual**		
	Acceleration	**Velocity**	**Displacement**
Two SMGAs	49.00	24.79	16.82
Three SMGAs	5.33	4.51	4.10
Four SMGAs	41.49	74.96	63.51

Figures 7, 8, 9(a), 10 and 11 show the comparisons between the observed records (see the bottom curves) and synthetic records (see the top curves) for the three components in velocity, acceleration, and displacement at the MANZ, CJIG, MOIG, ZAIG and ZIIG stations, respectively, for the best model with three SMGAs.

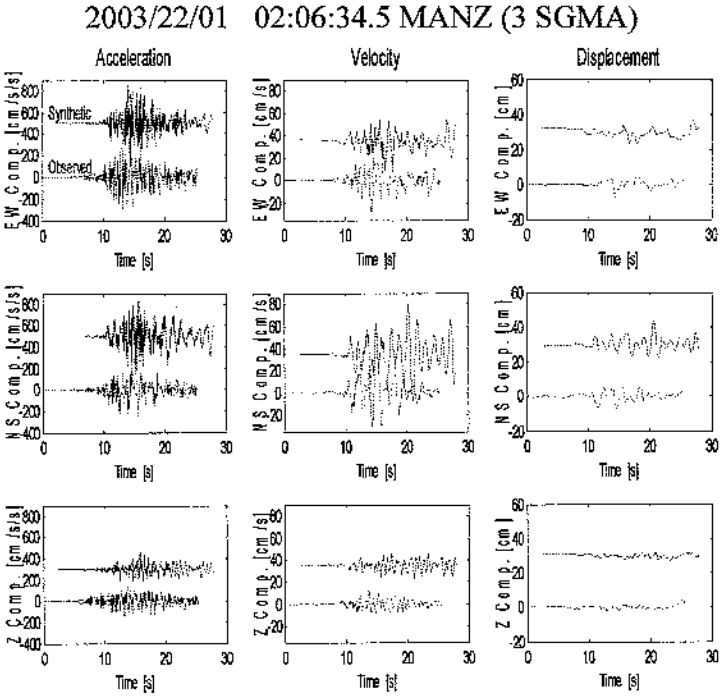

Fig. 7 Simulation for MANZ station with three SMGAs (top: synthetic; bottom: observed; columns from left to right: acceleration, velocity, and displacement; rows from top to bottom: EW, NS, and Z components)

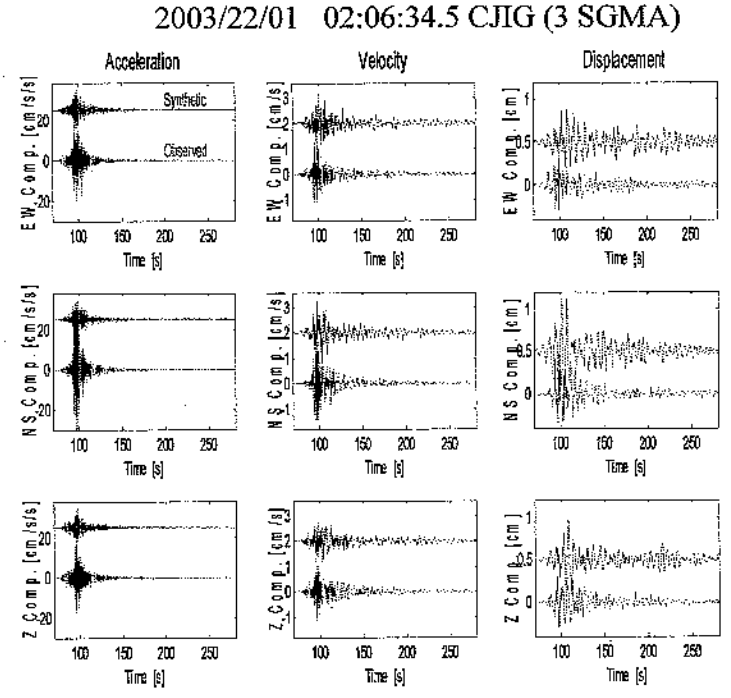

Fig. 8 Simulation for CJIG station with three SMGAs (top: synthetic; bottom: observed; columns from left to right: acceleration, velocity, and displacement; rows from top to bottom: EW, NS, and Z components)

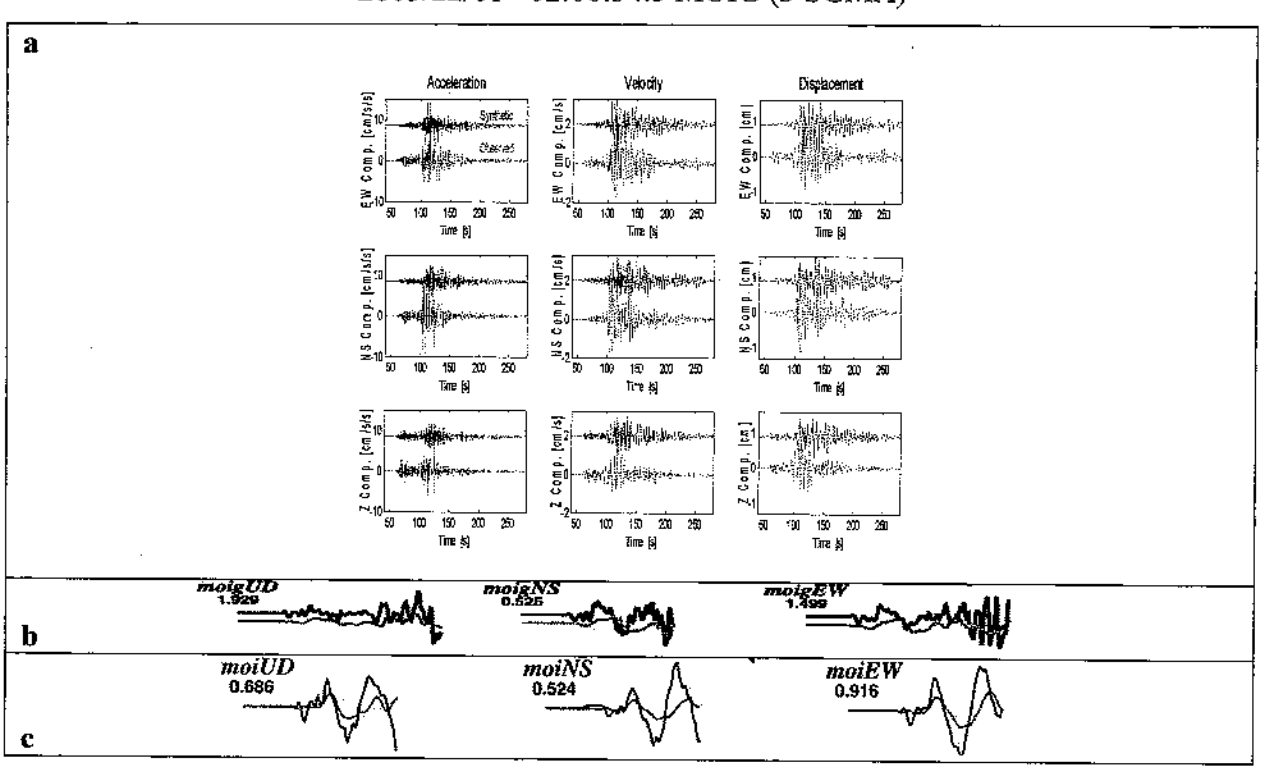

Fig. 9 (a) Simulation for MOIG station by the model with three SMGAs (top: synthetic; bottom: observed; columns from left to right: acceleration, velocity, and displacement; rows from top to bottom: EW, NS, and Z components); (b) Synthetic and observed records for the Tecomán earthquake at MOIG station from Yagi et al. (2004); (c) Synthetic and observed records for the Tecomán earthquake at MOIG station from Quintanar et al. (2010)

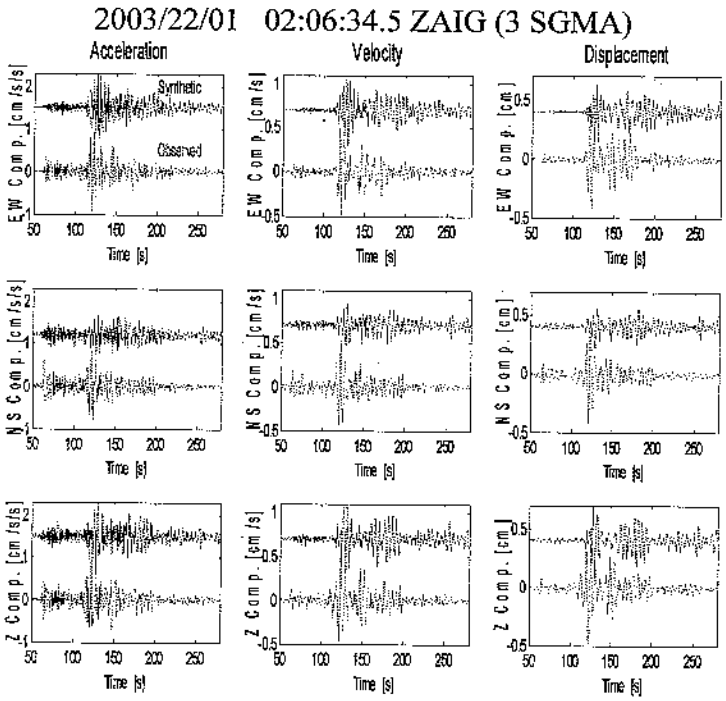

Fig. 10 Simulation for ZAIG station with three SMGAs (top: synthetic; bottom: observed; columns from left to right: acceleration, velocity, and displacement; rows from top to bottom: EW, NS, and Z components)

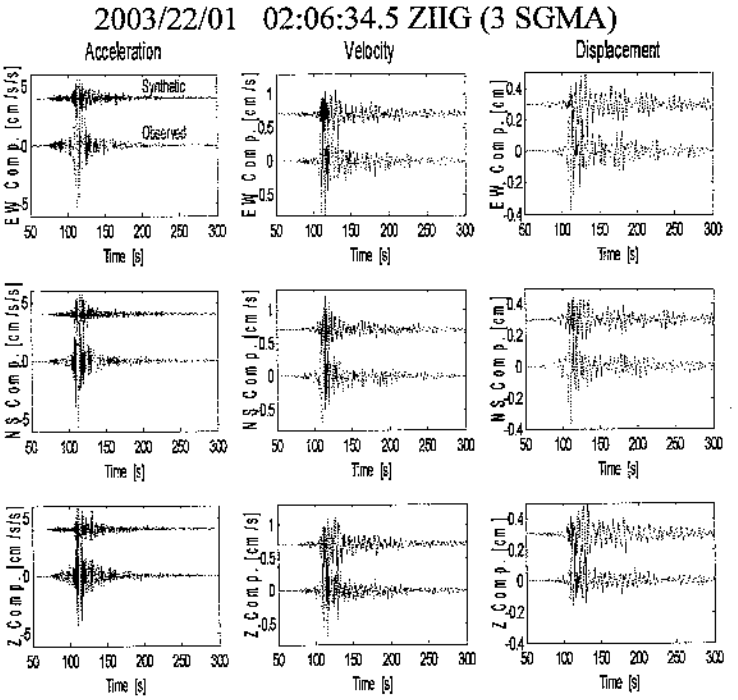

Fig. 11 Simulation for ZIIG station with three SMGAs (top: synthetic; bottom: observed; columns from left to right: acceleration, velocity, and displacement; rows from top to bottom: EW, NS, and Z components)

Figures 12–16 show the comparisons between the observed and synthetic Fourier spectra for the three components in velocity, acceleration, and displacement at the MANZ, CJIG, MOIG, ZAIG and ZIIG stations, respectively, for the best model with three SMGAs.

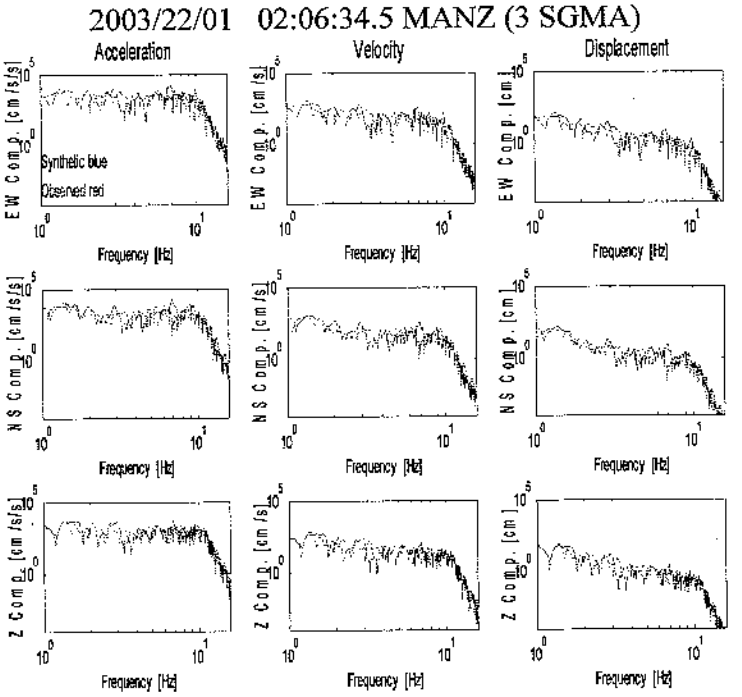

Fig. 12 Fourier spectra for MANZ station with three SMGAs (columns from left to right: acceleration, velocity, and displacement; rows from top to bottom: EW, NS, and Z components)

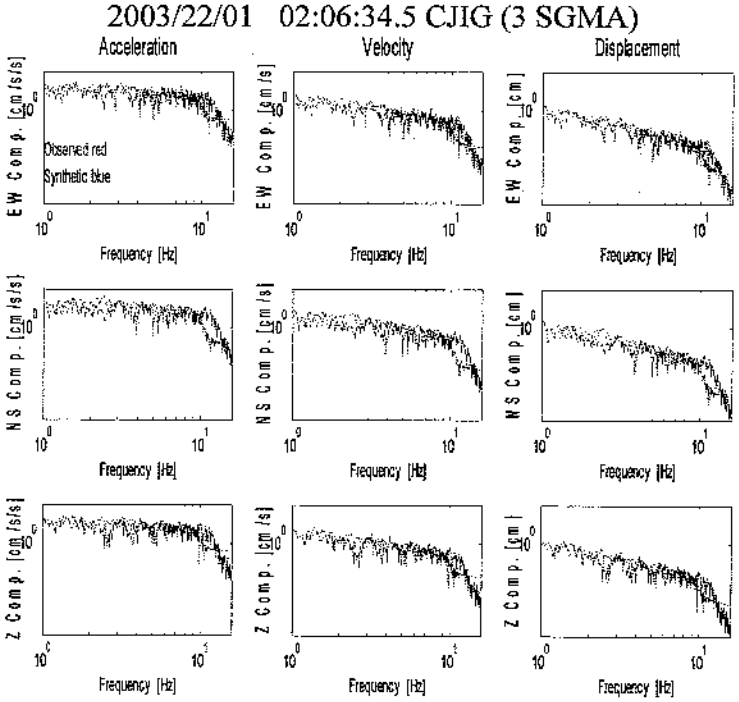

Fig. 13 Fourier spectra for CJIG station with three SMGAs (columns from left to right: acceleration, velocity, and displacement; rows from top to bottom: EW, NS, and Z components)

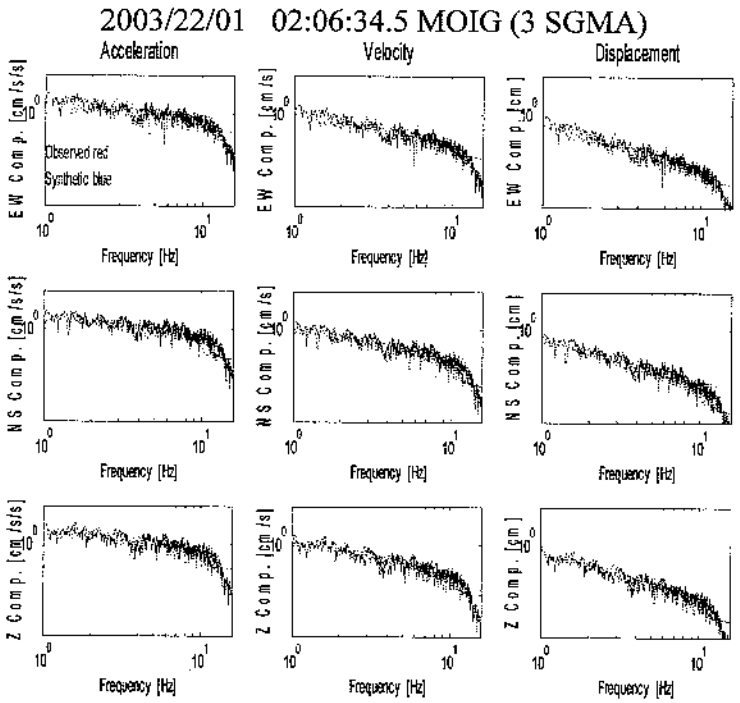

Fig. 14 Fourier spectra for MOIG station with three SMGAs (columns from left to right: acceleration, velocity, and displacement; rows from top to bottom: EW, NS, and Z components)

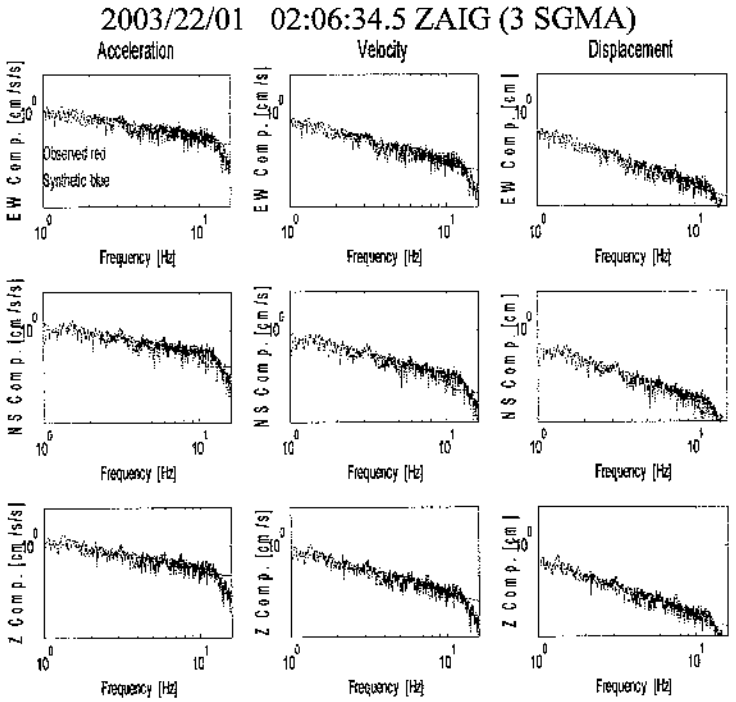

Fig. 15 Fourier spectra for ZAIG station with three SMGAs (columns from left to right: acceleration, velocity, and displacement; rows from top to bottom: EW, NS, and Z components)

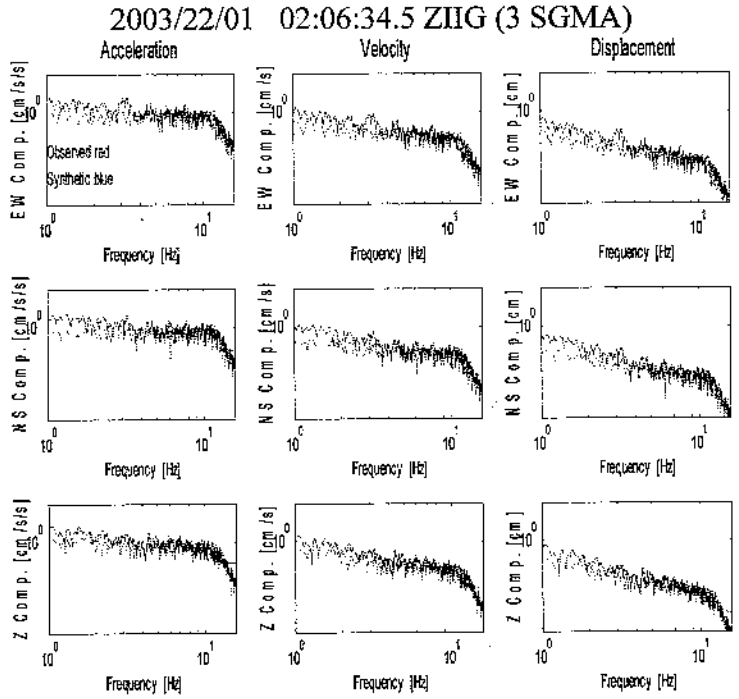

Fig. 16 Fourier spectra for ZIIG station with three SMGAs (columns from left to right: acceleration, velocity, and displacement; rows from top to bottom: EW, NS, and Z components)

Table 4 shows the best fit obtained for the model with four SMGAs. This model consists of the SMGA of 11.83 km^2, located 20.75 km SW of the epicenter; SMGA of 20.62 km^2, located 10.24 km SE

of the epicenter; SMGA of 35.50 km^2, located 20.16 km NE of the epicenter; and SMGA of 11.83 km^2 at 18.45 km SW of the epicenter.

For the spectral analysis conducted for the MANZ site, HVSPR were computed between each horizontal component and the vertical component in order to identify the local site effects using the weak (for microtremors), moderate (for the earthquake of M_W = 5.5), and strong (for the earthquake of M_W = 7.5) ground motions. Further, an analysis was conducted to provide an empirical evidence to support the hypothesis that for the frequency range of 1–10 Hz, nonlinear effects are significant at the MANZ soft soil site. In Figure 17, both H_{NS}/V and H_{EW}/V spectral ratios (SPR) are presented. In both graphs, the HVSPR of the strong and the moderate earthquake ground motions, as well as those for the microtremor ground motions, are also plotted for an easy viewing of the frequency shift to lower values. On inspecting, from the weak motions (see the dash-dot, dashed, and thick-dotted lines, all with maximum amplitude peaks around 0.7 Hz) to the moderate (see the thin solid line) and strong (see the dashed thin line) ground motions, two maximum amplitude peaks are clearly seen. One peak each can be observed at the frequencies of 4 and 3 Hz, respectively, for the H_{NS}/V SPR, and the second-maximum amplitude peaks for both earthquakes are located between 0.68 and 0.59 Hz. The H_{EW}/V SPR for the moderate earthquake ground motion exhibit a wide frequency range of 0.5–0.7 Hz, and the second-maximum amplitude peak for the strong earthquake ground motion is located between 0.8 and 0.9 Hz. On comparing the dotted line, which belongs to the CASA site (located on a rocky outcrop), with all other lines, the local site effects become clearly evident; however, the nonlinear response behavior is not evident. Details of the station identification and the corresponding line are provided in the caption of Figure 17.

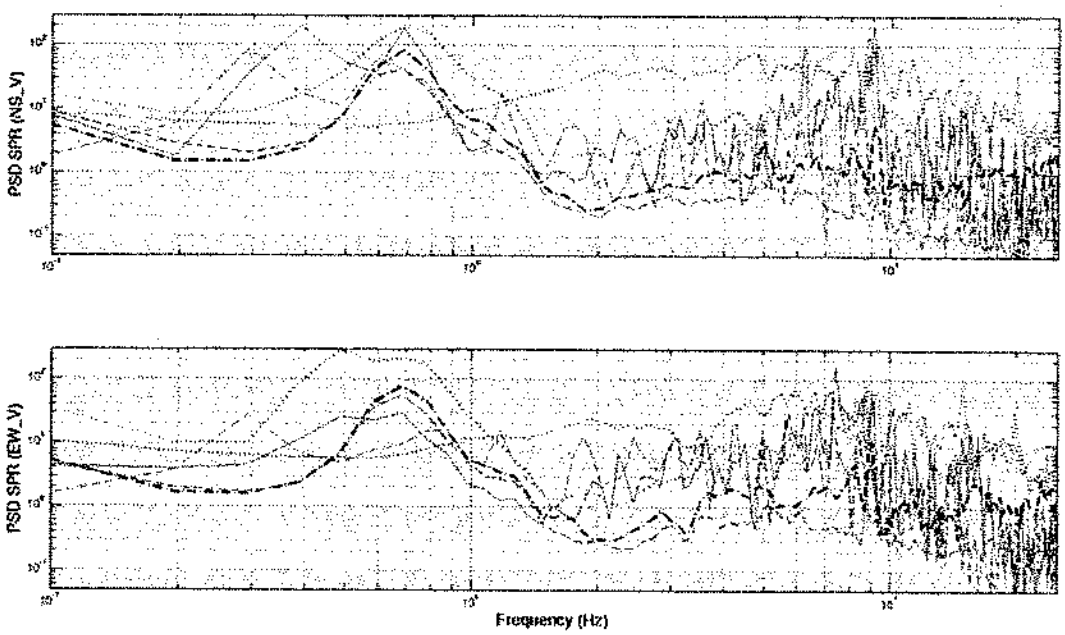

Fig. 17 Spectral ratios of microtremors, moderate and strong ground motions (top: H_{NS}/V SPR; bottom: H_{EW}/V SPR; the dashed-thin and solid-thin lines are for the strong (for the earthquake of M_W = 7.5) and moderate (for the earthquake of M_W = 5.5) ground motions, respectively, both recorded at the MANZ soft soil site; the small-dots line is for the CASA site on rocky outcrop; the dash-dot and dashed lines correspond to the CAMPOS and LAGOS soft-soil sites, respectively; the large-dots line belongs to the MANZ soft-soil site)

As mentioned before, the spectral analysis was done for the MANZ site to identify if significant nonlinear effects were present in the frequency band of 1–10 Hz. This was not necessary for the other four sites because those are located on hard rocks.

The non-significant effect of the nonlinear response of soft soils at the MANZ site is now well supported by the inspection of the frequency shift associated with no significant amplitude changes, as the HVSPR have demonstrated, at least for the frequency band of 1–10 Hz. On the other hand, the local site effects of the soft soils of our study area are also confirmed on comparing the HVSPR of the CASA site (located on a rocky outcrop) with those of the rest of the sites, which are located on soft soils.

As part of this investigation, we quantified individual and average characteristics of SMGA, rupture area, dislocation time and rise time. These values are related with the seismic moment of these events, M_0 (= 1.6×10^{20} N-m); the results obtained were compared with the relationships proposed by Somerville et al. (2002) for the subduction earthquakes (see Table 6). These relationships involved the seismic moment M_0 and the inner and outer parameters. The outer parameters are fault area, dislocation time, and rise time. The inner parameters are the total area of all SMGAs, the area of bigger SMGA, the radius of bigger SMGA, and the distance from hypocenter to the nearest SMGA.

Table 6: Comparison between the Relationships Proposed by Somerville et al. (2002) for Subduction Earthquakes and the Results of This Study

	This Study (A)	Somerville et al. (2002) (B)	Ratio (= A/B)
Rupture Area	5.95E+03	8.01E+03	7.43E-01
Dislocation Time	3.00E+01	4.80E+00	6.25E+00
Rise Time	4.00E-01	2.38E+00	1.68E-01
Total Area of SMGA	7.40E+01	2.00E+03	3.70E-02
Area of the Largest SMGA	3.55E+01	1.30E+03	2.73E-02
Radius of the Largest SMGA	3.36E+00	2.20E+01	1.53E-01
Hypocentral Distance of the Nearest SMGA	1.37E+01	2.10E+01	6.53E-01

The results of these comparisons show that the relationships between M_0 and rupture area, and M_0 and hypocentral distance to the nearest asperity, adjust moderately well. However, this is not the case for the rest of the relationships described above.

DISCUSSION

The best model obtained consists of three SMGAs of maximum dislocation. The process of finding the best adjustment mentioned above generated four different models (of one, two, three, and four SMGAs). This process clearly shows that the residual values for the local station MANZ decreased progressively (see Table 5). First, on modeling the target event with a single SMGA and on varying the location from Position A (with residual acceleration = 108.75) to Position B (with residual acceleration = 23.00), the residual value was reduced. The residual value improved significantly on modeling with two SMGAs (with residual acceleration = 6.13), at the locations shown in Figure 5(c). The best adjustment was obtained when the target event was modeled with three SMGAs, at the locations shown in Figure 5(d) (with residual acceleration = 4.79). However, when modeled with four SMGAs (see Figure 5(e)), the best model generated a residual of 6.82 and thus the residual increased. The poor adjustment with four SMGAs (which directly involves an increase in the area of SMGA) is evident on comparing the synthetic and observed records of Figure 18. The components of velocity and displacement have a similar behavior.

The model process includes the variation of other parameters like that of V_r and rise time. The parameters with major weights in the model are the number, sizes and locations of SMGAs. The optimal model is a combination of all these parameters. In order to find a minor residual that could increase the total area of SMGA, it is necessary to consider that the method used considers displacement in SMGA to be uniform. This is not completely correct. Displacements can vary inside an SMGA and can take significant weights in the fitting. Additionally, it is necessary to take into consideration the quantity and

quality of the available data. Nozu and Irikura (2008) used the same method to model the Tokachi-Oki 2003 earthquake. The K-NET and KiK Japan networks recorded this earthquake and aftershocks at 600 accelerographic stations. Forty stations with better azimuthal coverage were chosen for the modeling. In contrast, in this study we have only five stations, only one near the source (i.e., the MANZ station, located at a distance of 53.82 km to the hypocenter), and the other four with distances ranging from 132 km (for CJIG) to 494 km (for ZAIG). Despite the limited quantity and quality of available data, the comparison of residuals and the fitting between synthetic and observed records and their Fourier spectra show that residuals were considerably minimized.

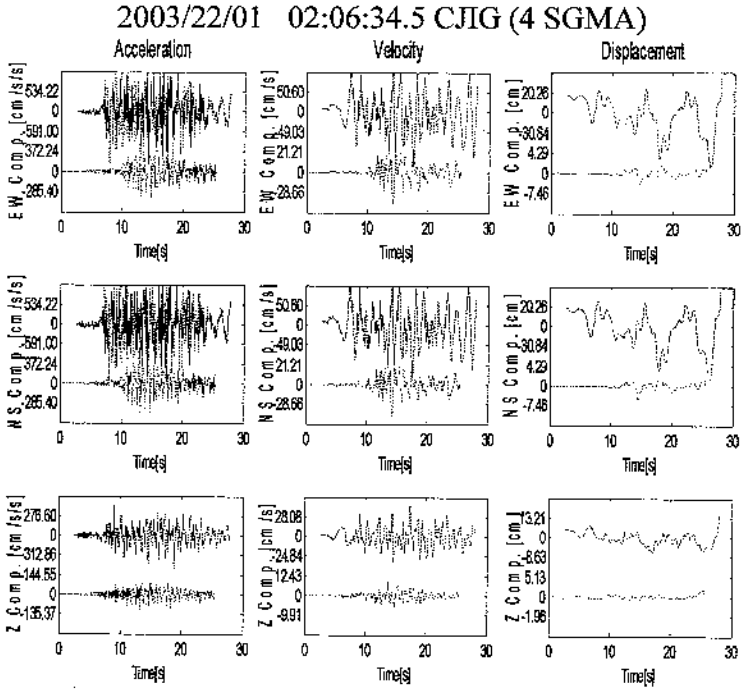

Fig. 18 Simulation for MANZ station with four SMGAs (columns from left to right: acceleration, velocity, and displacement; rows from top to bottom: EW, NS, and Z components; synthetic waveforms overestimate the observed waveforms)

Figure 9(a) shows, for the MOIG station, the adjustment between the synthetic and observed records at high frequencies, as obtained in this study for the Tecomán earthquake. Figures 9(b) and 9(c) show the adjustments at low frequencies obtained from the inversions of Yagi et al. (2004) and Quintanar et al. (2010), respectively. The poor adjustment at low frequencies for this station is attributed to the lack of cortical information for this site. Our results show contrasting results on applying the EGFM.

The final model with three SMGAs, having presented the best adjustment in residuals, also gives a close resemblance with the dislocation model found by Yagi et al. (2004) (see Figure 19), who reported that the rupture process is divided in three stages. In the first stage, the rupture starts near the hypocenter. In the second stage, the rupture propagates towards the southeast and breaks the asperity A, which is 15 km away from the starting point of the rupture; at the same time, a third stage occurs in which the rupture spreads to the northeast and breaks the asperity B, which is 25 km away from the starting point of the rupture. SMGA "1" in our model is located at 1.72 km from the center of asperity A, as reported by Yagi et al. (2004); SMGA "2" is located at 5.16 km from the hypocenter, and SMGA "3" is located at the same place as the asperity B, as reported by Yagi et al. (2004).

In Table 5 we can observe that the stations MANZ and ZAIG have adjustments better than 90% in the accelerations for the WE and Z components, and that adjustments in velocity are better than 70% for the same components; adjustments in acceleration, velocity and displacement for the NS component at the same stations are less than 60%. In the same way, adjustments in acceleration for the three components at the remaining stations (i.e., CJIG, MOIG and ZAIG) are less than 60%.

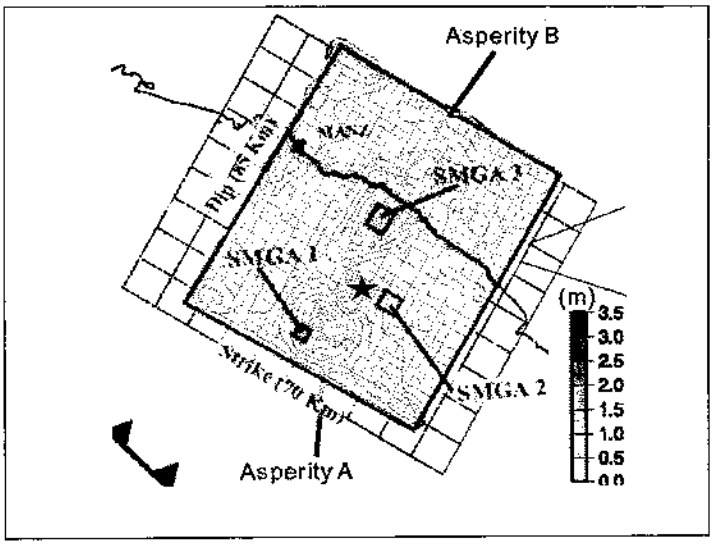

Fig. 19 Comparison between the dislocation model obtained by Yagi et al. (2004) and the positions and sizes of the SMGAs generated with our model

Singh et al. (2003) show that the Tecomán earthquake of 2003 generated directivity in the direction of the station COIG, which then spread to Colima city and to the northeast with an azimuth of 38°NE. The stations which presented the best adjustments in acceleration, velocity and displacement (i.e., the stations MANZ and ZAIG) seem to fit this direction of rupture propagation of the earthquake. The stations, where the adjustments were smaller that 50% (i.e., the stations CJIG, MOIG and ZIIG), seem to be outside this direction. The Tecomán earthquake of 2003 originated in the center of El Gordo graben and spread in the direction mentioned above within the Colima State. The peak values in accelerations, velocities, and displacements at the stations that are outside the direction of rupture propagation of the earthquake might be explained due to a phenomenon wherein the boundaries of the graben operate as borders and the seismic waves undergo diffraction, reflection, and refraction at those borders. This implies that the direction, in which the waves propagate after arriving at this border, depends on their initial trajectory. This further means that the direction of wave propagation depends on the location of the earthquake within the graben. Thus, in order to reproduce waveforms at the stations outside the graben (perpendicular to the direction of propagation), the locations of the target and element events should be as close as possible. However, the distance between these two earthquakes is 36 km. The adjustments in the peak values in acceleration, velocity, and displacement for the stations that are outside the direction of rupture propagation are not clear in comparison with the good adjustments for the stations that are located in this direction.

From the interpretation of the results of the spectral analysis, we conclude that the nonlinear effects of soft soils were not significant at the MANZ site. This is well supported by the mild frequency shift seen in the HVSPR plots, at least for the frequency band of 1–10 Hz. On the other hand, the local site effects of soft soils in our study area are also confirmed on comparing the HVSPR of the CASA site (on rocky outcrop) with those of the rest of the sites (located on soft soils).

We applied the relationships proposed by Somerville et al. (2002) for subduction earthquakes, which related seismic moment with some source parameters, as well as seismic moment with some characteristics of the SMGA generated in this study (see Table 6). The results show that the relationship between M_0 and hypocentral distance to the nearest asperity gets adjusted by 53% to the value proposed by Somerville et al. (2002). The number of SMGAs in our model is 3, which is close to 2.4 proposed by Somerville et al. (2002). However, when the relationship between M_0 and rupture area is compared, the area obtained in the inversion made by Yagi et al. (2004) is only 27% of the value proposed by Somerville et al. (2002). For the same relation, Quintanar et al. (2010) obtained an area of 22.40% of the value proposed by Somerville et al. (2002). Garduño (2006) applied the same relationships to her model obtained for the July 15, 1996 earthquake in the Guerrero State coast. When she applied the relationship between M_0 and rupture area, the obtained value was only 3% of that proposed by Somerville et al. (2002). For the rest of the relationships the values obtained with our model are usually less than 15%

of those obtained by Somerville et al. (2002). The results obtained by Yagi et al. (2004), Quintanar et al. (2010), Garduño (2006) as well as those obtained in this study suggest that not all of the relationships proposed by Somerville et al. (2002) are applicable to the subduction zone in Mexico.

CONCLUSIONS

In this investigation, we have generated a model for the Tecomán earthquake of January 22, 2003, while applying the method of empirical Green's functions and using the acceleration records of two earthquakes. The Tecomán earthquake has been used as the target event and the November 21, 2006 event as the element event. We have used the acceleration data recorded at the MANZ station, as obtained by CIRES, and the velocity data of four broad-band regional stations of SSN. These four stations provided good azimuthal coverage of the Tecomán earthquake. The process of modeling the target event has been done in four stages involving one, two, three and four SMGAs, respectively. The observed waveforms have been adjusted gradually by the synthetic waveforms and the residual values have progressively decreased in each stage from one to three SMGAs; the model with four SMGAs has shown an increased value in residual values and poor adjustment. Thus, the best fitting has been obtained by modeling the target event with three SMGAs, corresponding to the best adjustment in residual values. In addition, this model has a close resemblance with the dislocation model found by Yagi et al. (2004). The SMGA "1" found in our model is located at 1.72 km from the asperity A, as reported by Yagi et al. (2004). SMGA "2" is located at 5.16 km away from the hypocenter, and SMGA "3" is located at the same place as the asperity B found by Yagi et al. (2004).

We conclude that for the frequency band of 1–10 Hz, the nonlinear effects of soft soils were not significant at the MANZ site. The mild frequency shift seen on the HVSPR plots supports our interpretation. On the other hand, local site effects, due to soft soils, have been confirmed by comparing the HVSPR for all recording sites.

ACKNOWLEDGEMENTS

We thank three anonymous reviewers and the Editor for their constructive comments. We appreciate the support of Lucio Camarillo of Centro de Instrumentación y Registro Sísmico (CIRES), for providing the acceleration records of the MANZ station, and the support of Carlos Valdés González, Caridad Cárdenas, for providing the records of the broadband network of Servicio Sismológico National (SSN). This experiment could have not taken place without the valuable help of Ricardo Vasquez, Horacio Mijares Juan Tejeda Jacome and Miguel Rodriguez in the instrumentation and logistic support. We thank Consejo Nacional de Ciencia y Tecnología (CONACYT) for the support provided to this project (under Grant No. SEP-2003-C02-43880/A).

REFERENCES

1. Aki, K. (1967). "Scaling Law of Seismic Spectrum", Journal of Geophysical Research, Vol. 72, No. 4, pp. 1217–1231.
2. Aki, K. (1988). "Local Site Effects on Strong Ground Motion" in "Earthquake Engineering and Soil Dynamics II—Recent Advances in Ground-Motion Evaluation (edited by J.L. Von Thun)", Geotechnical Special Publication 20, American Society of Civil Engineers, New York, U.S.A.
3. Aki, K. (1993). "Local Site Effects on Weak and Strong Ground Motion", Tectonophysics, Vol. 218, No. 1-3, pp. 93–111.
4. Alcocer, S.M. and Klingner, R.E. (editors) (2006). "The Tecomán, México Earthquake January 21, 2003: An EERI and SMIS Learning from Earthquakes Reconnaissance Report", Technical Report, Earthquake Engineering Research Institute, Oakland, U.S.A.
5. Bandy, W., Mortera-Gutierrez, C., Urrutia-Fucugauchi, J. and Hilde, T.W.C. (1995). "The Subducted Rivera-Cocos Plate Boundary: Where is It, What is It, and What is Its Relationship to the Colima Rift?", Geophysical Research Letters, Vol. 22, No. 22, pp. 3075–3078.
6. Bendat, J.S. and Piersol, A.G. (1971). "Random Data: Analysis and Measurement Procedures", John Wiley & Sons, Inc., Hoboken, U.S.A.

7. Chang, S.W. and Bray, J.D. (1998). "Implications of Recent Strong Motion Data for Seismic Building Code Design at Deep, Stiff Soil Sites", Proceedings of the NEHRP Conference and Workshop on Research on the Northridge, California Earthquake of Janurary 17, 1994, Richmond, U.S.A., Vol. II, pp. 90–99.
8. Field, E.H., Johnson, P.A., Beresnev, I.A. and Zeng, Y. (1997). "Nonlinear Ground-Motion Amplification by Sediments during the 1994 Northridge Earthquake", Nature, Vol. 390, No. 6660, pp. 599–602.
9. Finn, L.D. (1991). "Geotechnical Engineering Aspects of Microzonation", Proceedings of the Fourth International Conference on Seismic Zonation, Stanford, U.S.A., Vol. 1, pp. 199–259.
10. Garduño, N. (2006). "Procesos de la Fuente del Sismo del 15 de Julio de 1996 Usando el Método de la Función de Green Empírica y Algoritmos Genéticos", Licenciate Thesis, Facultad de Ingeniería, Universidad Nacional Autónoma de México, Mexico City, Mexico (in Spanish).
11. Idriss, I.M. (1990). "Response of Soft Soil Sites during Earthquakes", Proceedings of H. Bolton Seed Memorial Symposium, Berkeley, U.S.A., Vol. 2, pp. 273–289.
12. Irikura, K. (1986). "Prediction of Strong Acceleration Motions Using Empirical Green's Function", Proceedings of the Seventh Japan Earthquake Engineering Symposium, Tokyo, Japan, pp. 151–156.
13. Kanasewich, E. (1981). "Time Series Analysis in Geophysics", University of Alberta Press, Edmonton, Canada.
14. Milne, J. (1898). "Seismology", Kegan Paul, Trench, Trübner & Co. Ltd., London, U.K.
15. Miyake, H., Iwata, T. and Irikura, K. (2003). "Source Characterization for Broadband Ground-Motion Simulation: Kinematic Heterogeneous Source Model and Strong Motion Generation Area", Bulletin of the Seismological Society of America, Vol. 93, No. 6, pp. 2531–2545.
16. Nozu, A. and Irikura, K. (2008). "Strong-Motion Generation Area of a Great Subduction-Zone Earthquake: Waveform Inversion with Empirical Green's Functions for the 2003 Tokachi-Oki Earthquake", Bulletin of the Seismological Society of America, Vol. 98, No. 1, pp. 180–197.
17. Oppenheim, A.V. and Schafer, R.W. (1975). "Digital Signal Processing", Prentice-Hall, Englewood Cliffs, U.S.A.
18. Quintanar, L., Rodríguez-Lozoya, H.E., Ortega, R., Gómez-González, J.M., Domínguez, T., Javier, C., Alcántara, L. and Rebollar, C.J. (2010). "Source Characteristics of the 22 January 2003 M_w = 7.5 Tecomán, Mexico, Earthquake: New Insights", Pure and Applied Geophysics (in press).
19. Reid, H.F. (1910). "The California Earthquake of April 18, 1906—Report of the State Earthquake Investigation Commission in Two Volumes and Atlas, Volume II: The Mechanics of the Earthquake", Publication 87, Volume II, Carnegie Institute of Washington, Washington, DC, U.S.A.
20. Seed, H.B. and Idriss, I.M. (1982). "Ground Motions and Soil Liquefaction during Earthquakes", Monograph MNO-5, Earthquake Engineering Research Institute, Oakland, U.S.A.
21. Singh, S.K., Ponce, L. and Nishenko, S.P. (1985). "The Great Jalisco, Mexico, Earthquakes of 1932: Subduction of the Rivera Plate", Bulletin of the Seismological Society of America, Vol. 75, No. 5, pp. 1301–1313.
22. Singh, S.K., Pacheco, J.F., Alcántara, L., Reyes, G., Ordaz, M., Iglesias, A., Alcocer, S.M., Gutierrez, C., Valdés, C., Kostoglodov, V., Reyes, C., Mikumo, T., Quaas, R. and Anderson, J.G. (2003). "A Preliminary Report on the Tecomán, Mexico Earthquake of 22 January 2003 (M_w 7.4) and Its Effects", Seismological Research Letters, Vol. 74, No. 3, pp. 279–289.
23. Somerville, P., Irikura, K., Graves, R., Sawada, S., Wald, D., Abrahamson, N., Iwasaki, Y., Kagawa, T., Smith, N. and Kowada, A. (1999). "Characterizing Crustal Earthquake Slip Models for the Prediction of Strong Ground Motion", Seismological Research Letters, Vol. 70, No. 1, pp. 59–80.
24. Somerville, P.G., Sato, T., Ishii, T., Collins, N.F., Dan, K. and Fujiwara, H. (2002). "Characterizing Heterogeneous Slip Models for Large Subduction Earthquakes for Strong Ground Motion Prediction", Proceedings of the 11th Japan Earthquake Engineering Symposium, Tokyo, Japan, pp. 163–166 (in Japanese).
25. Yagi, Y., Mikumo, T., Pacheco, J. and Reyes, G. (2004). "Source Rupture Process of the Tecomán, Colima, Mexico Earthquake of 22 January 2003, Determined by Joint Inversion of Teleseismic Body-

Wave and Near-Source Data", Bulletin of the Seismological Society of America, Vol. 94, No. 5, pp. 1795–1807.

26. Zobin, V.M. and Pizano-Silva, J.A. (2007). "Macroseismic Study of the M_w 7.5 21 January 2003 Colima, México, Across-Trench Earthquake", Bulletin of the Seismological Society of America, Vol. 97, No. 4, pp. 1221–1232.

---

[1] Website of CMT, www.seismology.harvard.edu/CMTsearch.html